

## OSL EQUIVALENT DOSE

### Preparation and measurement procedure

Under subdued orange lighting, samples were sieved to obtain the 180-212  $\mu\text{m}$  grain size fraction, which was then treated with HCl, H<sub>2</sub>O<sub>2</sub>, and HF to isolate the quartz. Sub-samples were prepared for measurement by placing roughly 100-200 grains on small steel discs. OSL measurements were performed on three Risø TL/OSL-DA-15 Readers (Bøtter-Jensen et al., 2000), using optical stimulation power of  $\sim 30 \text{ mWcm}^{-2}$  at a wavelength of 470 nm (blue light). The detection filter was a 7.5 mm Hoya U340, with transmission between 270-380 nm. An inbuilt  $^{90}\text{Sr}/^{90}\text{Y}$  source provided a dose rate of either  $\sim 0.03$  or  $\sim 0.13 \text{ Gys}^{-1}$ .

### Protocol

Our protocol for estimating the Equivalent dose ( $D_e$ ) is based on the Single Aliquot Regenerative dose (SAR) protocol of Murray and Wintle (2000). The samples are relatively young (mostly 100 - 400 a), returning  $D_e$  of 0.2 - 0.5 Gy. The dating of such young samples introduces several complications which are less relevant for most OSL dating studies: 1. the weakness of the OSL signal; 2. the susceptibility of the signal to unwanted thermal transfer of charge; and 3. the possibility of partial bleaching. Overcoming these issues required us to introduce certain methodological adaptations, as follows:

1. Weak signals lead to less precise measurements, and it therefore requires the processing of a large number of aliquots to arrive at a satisfactory precision in  $D_e$ . Increasing the aliquot size is undesirable, as it becomes more likely that unbleached grains, or grains otherwise unsuitable for dating, are included in the aliquot. To increase the number of aliquots processed, we constructed the dose response curve for each aliquot using a single regenerative dose point (Ballarini et al., 2007). While reducing measurement time per aliquot, this adaptation leads to an overestimate of  $D_e$  of  $\sim 1\%$  (assuming that the true dose-response curve conforms to a typical saturating exponential function). We consider this overestimate to be insignificant compared to other sources of error.
2. Young samples are susceptible to thermal transfer effects, because the small natural signals can be easily swamped. We attempted to minimise thermal transfer by choosing a relatively low preheat, selected using a thermal-transfer test (Wallinga et

al., 2010). The effects of high preheats can be seen in Fig. DR1 (thermal-transfer test) and Fig. DR2. (Preheat-plateau test). Furthermore, we used an additional OSL bleach at elevated temperature at the end of each SAR cycle (see Table DR1), which was found by Murray and Wintle (2003) to reduce recuperation.

3. Partial bleaching occurs when the mineral grains receive too little optical exposure (from sunlight) during transport and deposition. Young samples are more susceptible to this phenomenon, because of the relatively small burial signal. Most of the samples in this paper were deposited through beach/aeolian mechanisms, and are very likely to be well-bleached. However, several samples were taken directly from storm-surge sediments, for which the bleaching conditions are more debatable. To maximize the chances of obtaining a well-bleached OSL signal, we used the ‘Early Background’ principal of selecting integration intervals (Cunningham and Wallinga, 2010). In this method, the OSL signal is taken from the initial portion of the OSL decay curve, with the background taken from the portion immediately following. By keeping the length of the background interval to roughly 2.5 times that of the initial signal, a high proportion of easily-bleachable ‘fast’ component is achieved, while maintaining a good signal-to-noise ratio. The time-intervals we used were 0 – 0.60 s for the initial signal, and 0.60 – 2.10 s for the background. Errors arising through counting statistics were calculated using the equation of Li (2007), for use with weak signals.

Three tests were included in our protocol to verify the suitability of each aliquot for dating. Firstly, the OSL response to a ‘zero’ dose was measured, with aliquots accepted if the dose was less than 0.05 Gy or overlapping zero within one standard error. A ‘recycle’ dose was given, with aliquots accepted if the recycling ratio was between 0.9 and 1.1. A second recycling ratio was measured, with the same acceptance criteria, but following an infrared bleach at room temperature. This was used to identify any remnant feldspar contamination. We used the Central Age Model (CAM) of Galbraith et al. (1999) to estimate  $D_e$  for each sample. The SAR Protocol we used varied slightly between different site locations, as detailed in Table DR1. To test the suitability of the protocols, dose-recovery tests were carried out on all samples. The combined results for all samples are shown in Fig. DR3, which has a central dose-recovery ratio (using the CAM) of  $0.997 \pm 0.005$ , and overdispersion ( $\sigma$ ) of  $2.2 \pm 0.7$  %.

### **Partial Bleaching**

Two storm-surge samples (HK1-16 and ZN1-4) gave anomalously old ages when processed with the central age model. One explanation for this could lie in the nature of deposition, through which the grains may not have received sufficient sunlight to fully reset the OSL signal. This ‘partial bleaching’ would lead to age overestimates if not accounted for. To determine whether the two samples are affected, we calculated the sample ages using two combinations of OSL decay curve integration intervals.

Cunningham and Wallinga (2010) argued that for partially bleached samples, the use of ‘early background’ integration intervals should lead to a reduction in scatter in  $D_e$  when compared to the ‘late background’ intervals, due to the reduced proportion of hard-to-bleach slow component in the net OSL signal. To investigate the bleaching, we ran the CAM to determine the overdispersion on both samples, using both the late and early background integration intervals.

For sample ZN1-4, it can be seen in Table DR2 that the use of the late background leads to an increase in both  $D_e$  and  $\sigma$ , as would be expected from a partially bleached sample. In addition,  $\sigma$  calculated using the Early Background is significantly larger than found in the surrounding samples (see Table DR3.), implying that an additional source of scatter (most likely partial bleaching) is present. For this sample we calculated the age using the 3-parameter minimum-age model (MAM3) of Galbraith et al. (1999). The MAM3 requires a specified  $\sigma$ , for which we used the well-defined value of 10% derived from well-bleached sample ZN1-2.

For sample HK1-16, it is apparent from Table DR2 that little change in  $D_e$  or  $\sigma$  occurs when different integration intervals are used. Furthermore, the early-background derived  $\sigma$  of 17% is similar to those of the surrounding samples, shown in Table DR3. We cannot rule out partial bleaching as a source of error for this sample, but we can find no evidence to support that hypothesis other than the anomalously old age estimate. For this sample, we use the CAM to derive the age, and treat it as an unexplained outlier.

## THE DOSE RATE TO QUARTZ GRAINS

Measurements for determining the dose rate to quartz grains were made on the light-exposed end-sections of the sample tubes. Samples were homogenized by grinding, and the radionuclide concentration was determined through high-precision gamma-spectrometry. The dose rate ( $\dot{D}$ ) to the grains was estimated according to standard conversion factors for grain size (Mejdahl, 1979), water and organic content (assumed to be  $5 \pm 2\%$ ) (Aitken, 1998), and including an internal alpha contribution of  $0.01 \text{ Gy ka}^{-1}$  (Vandenberghe et al., 2008). With the exception of the shell-rich samples described below, dose rate calculations assume an infinite and uniform sediment matrix.

### The cosmic dose

The contribution of cosmic radiation to  $\dot{D}$  depends largely on the depth of the sample. For our samples this was made complicated by the build-up and movement of the overlying dunes, which may have altered the sample depth over time. Moreover, the depth of the sample just prior to sample collection was also uncertain because of erosion of the dune cliffs during the storm surge of 2007. We used two sources of information to help make an adequate approximation of the cosmic dose rate. Firstly, the approximate OSL ages of samples overlying the storm-surge sediment (this is only slightly circular,

since the cosmic-dose contribution to the total dose rate is usually less than 10%). Secondly, we make use of 'Jarkus' cross-shore profiles of the area. These profiles have been carried out roughly every 10 years since 1965, at 500 m intervals along coastline of the Netherlands. One profile was measured just prior to the storm surge of 2007 (Fig. 2).

HK1 and HK3 – for these sections the nearest Jarkus profiles indicate approximately 12 m of sediment above the storm surge unit, stable over the period 1965 - 2008. For the cosmic dose calculations, we assumed a gradual dune build-up to 12 m until 1965, and a constant depth of 12 m for 1965 - 2009.

HK7 – Jarkus profiles for this section indicate ~12 m of overlying sediment in 1965, reduced to 4 m in 2007. For our calculations, we assumed a gradual dune build-up to 12m until 1965, and a constant depth of 8.5 m from 1965-2009.

ZN1 – This inland site is situated in a dune low, with the storm surge unit < 1 m below the surface. The sample depth is unlikely to have changed since deposition, and the overlying sample indicates an age ~1800 AD. We therefore assumed an instant burial to its present depth.

Uncertainty in the sample depth inevitably leads to error in the age calculations. However, since the Jarkus profiles give evidence for dune stability over the last 50 years, and given the small contribution of cosmic dose to the total dose (~10 %), the actual error resulting from cosmic-dose uncertainty is unlikely to be significant.

### **The gamma dose**

Estimates of the gamma contribution to the dose rate for each sample are calculated from the measured radionuclide concentrations, using the infinite matrix assumption. However, for shell-rich or hash-rich samples HK3-4, HK3-5 and HK7-6, this assumption is not valid because the sedimentary units they come from are relatively thin (10-15 cm), and have a lower radionuclide concentration than the bracketing sediment. For these samples, we applied an upward correction of the gamma dose rate, using the gamma gradient estimates of Aitken (1985) in combination with the measured radionuclide concentrations of the bracketing sediment.

### **The beta dose**

For most samples, we use the 'infinite matrix' assumption when converting the measured radionuclide concentration into  $\dot{D}$ , and we further assume that the activity distribution is uniform throughout the sample. However, should there be discrete, non-radioactive material present, of a size comparable to (or greater than) the mean range of the typical beta particles (~1 mm), then the assumption of a uniform matrix becomes invalid. This has occurred for two samples taken directly from the storm-surge sediment (HK3-4, HK3-5), where significant amounts of marine shell are present; and one sample with significant proportion a fine shell fragments, or 'hash' (HK7-6). Gamma spectrometry

measurements indicated that a sample of pure shell would provide a beta dose rate to quartz grains of  $0.025 \text{ Gy ka}^{-1}$ , compared to roughly  $0.70 \text{ Gy ka}^{-1}$  typical of sandy samples. In addition, the density of the shell ( $\sim 2.70 \text{ g cm}^{-3}$ ) is significantly higher than the density of the sandy matrix in which the quartz grains are embedded ( $\sim 1.82 \text{ g cm}^{-3}$ , assuming porosity of 35 %). The shells create a low dose-rate zone in the sediment, within which no quartz grains exist. Measurements of radionuclide concentration are carried out on the bulk sediment (including the shells), which presents two complications. Firstly, the shells create a low dose-rate zone in the sediment within which no quartz grains exist; the quartz grains are found in the surrounding sand, which has more typical radionuclide concentrations. Secondly, the high density of the shells means they are better absorbers of radiation than sand grains of the same bulk volume; the beta dose must therefore be lower than a pure sand sample.

The net influence of the shell material on the beta dose rate is determined by the size, shape, and density of the shell material, and by the energy of the beta electrons. To estimate the average beta dose to quartz grains in the shell-rich environments, we used a Monte Carlo transport code, MCNP4C (Briesmeister, 2000). This code enables the generation of beta electrons of specified energy, and tracks them through a pre-defined geometry. Previous studies have shown that MCNP4C allows for accurate beta particle dose calculations in heterogeneous media (Schaart et al., 2002a; Schaart et al., 2002b; Maigne et al., 2011).

Two geometries were constructed: Model A, to simulate the shell-rich storm-surge deposit from which samples HK3-4 and HK3-5 were taken; Model B to simulate the hash-rich, pre storm-surge sample HK7-6. The two geometries varied only in the size and shape of the shell material, and the weight fraction of shell material. Visualisations of the two geometries are shown in Fig. DR4.

Geometries are based on a simple grid structure, in which shells and hash are rectangular cuboids of a sizes corresponding to the average (measured) shell size or hash size. Each shell fragment occupies one 'cell' of the geometry, and is composed of  $\text{CaCO}_3$  with density  $2.70 \text{ g cm}^{-3}$ . Shell cells were added to the geometry at random locations, using one of two orientations, until the (mass corrected) volume of shell material reached the desired fraction. All other space in the geometry is defined as a single cell, and represents the sand-matrix in which quartz grains are contained. The sand matrix material is a combination of  $\text{SiO}_2$  (i.e. quartz, density =  $2.66 \text{ g cm}^{-3}$ ) with a packing density of 65 % (typical for coarse sand deposits, Weerts, 1996); and  $\text{H}_2\text{O}$ , density =  $1.00 \text{ g cm}^{-3}$ , with mass equalling 5 % of the mass of the quartz. When combined, the density of the sand matrix is  $1.82 \text{ g cm}^{-3}$ . Air is ignored in the models; the low density of air ( $\sim 0.0013 \text{ g cm}^{-3}$ ) compared with solid materials means that the interaction of beta electrons with air is not significant in our models.

The energy of each beta electron is randomly sampled from a customised spectrum for each material (sand matrix or shell; Fig. DR5). These were created using the

measured radionuclide concentrations (Table DR4) in combination with the isotope-specific beta spectra, downloaded from [www.doseinfo-radar.com](http://www.doseinfo-radar.com). Charged particle equilibrium was maintained by specifying ‘white’ surfaces at the boundaries of the geometry, which reflect charged particles back into the model in random directions. The large sand matrix cell acts as the dosimeter, for which the average energy deposited per history is recorded using the \*F8 energy deposition tally (Briesmeister, 2000). All simulations were performed in coupled photon-electron mode, using the el03 and mcnp1b2 electron and photon interaction data libraries and selecting the ITS electron energy indexing algorithm (Schaart et al., 2002a). The upper photon and electron energy limits were set to 3.0 MeV. The photon and electron cut-off energies were set to 1 keV and 10 keV, respectively. Other simulation parameters were left at the default setting. No variance reduction techniques were applied.

To apply the model output to the measured beta dose rate, we define a correction factor:

$$r = \frac{E_{sand}}{E_{total}} \cdot \frac{m_{sand}}{m_{total}}$$

where  $E_{sand}$  is the energy deposited in the sand matrix as recorded in the \*F8 tally,  $E_{Total}$  is to total energy released,  $m_{sand}$  is the mass of the sand-matrix material, and  $m_{total}$  is mass of all the material. The ratio  $r$  reflects the dose absorbed by the sand matrix relative to the energy emitted per unit mass of bulk sediment. The true dose rate applicable to the quartz grains is found by correcting the measured bulk beta dose rate by the factor  $r$ .

### ***Model Results***

The computational time required for the models is short, because each model has only one, large dosimeter. For Model A (shells),  $r = 1.31$ , with a relative statistical error of 0.35 % ( $1\sigma$ ) after 154,000 particle histories; for Model B (hash),  $r = 1.17$ , with a relative statistical error of 0.45 % ( $1\sigma$ ) after 99,000 particle histories. To estimate the overall uncertainty associated with  $r$  (i.e., including possible systematic errors), we conducted a series of sensitivity tests in which  $r$  is modelled, for both geometries, while three key parameters are varied. The outcomes of the sensitivity tests are shown in Fig. DR6, and are discussed in the following paragraphs.

The parameter with the largest influence on  $r$  is the shell content (Fig. DR6 (a) and (b)). The more shell material in the sample, the greater the correction factor. When the proportion of shell material is low, the response of the correction factor is roughly linear; when the proportion of shell mass is increased beyond ~20%, the chance increases that more than one shell is located close enough to a given sand grain to absorb part of the beta energy emitted by that grain, leading to a steeper curve. The shell content of our samples was measured directly (28% for HK3-4 and HK3-5, 30% for HK7-6). An

estimated uncertainty of 3 % on the shell content leads to an uncertainty in  $r$  of roughly 0.03.

The influence of packing density of the sand-matrix material can be seen in Fig. DR6 (c) and (d). Unlike the shell mass, the packing density of the sand-matrix material was not measured. For our models we use a packing density 65 %, which was determined by Weerts (1996) to be typical for coarse sand. While there is clearly uncertainty over this value (estimated here as 5 %) it is also clear from Fig. DR6 (c-d) that an error in the packing density will not significantly affect the value of  $r$ .

Lastly, the sensitivity of  $r$  to a change in the volume of individual shells (or shell fragments) is displayed in Fig. DR6 (e-f). As with the sensitivity to packing density, a small error in individual shell volume has little effect on  $r$ . It is interesting to note, however, that even with a very small volume for each shell (e.g. a grain of 1 mm diameter), there is a considerable effect on  $r$ . As such this is not surprising given that the range of the beta particles is also in the order of millimetres. However, the implication is that even small non-emitting objects may affect the pattern of energy deposition, with the magnitude of the effect controlled by the proportion of that material in the sediment. This result could have implications for wider OSL dating, and is worthy of further investigation.

In summary, the known uncertainties in the beta-dose models are very small, and are barely significant when added to other sources of error in the age estimates. The correction values we use are  $1.31 \pm 0.05$  for Model A (Shells, samples HK3-4 and HK3-5), and  $1.17 \pm 0.05$  for Model B (Hash, HK7-6).

## REFERENCES

- Aitken, M.J., 1985, *Thermoluminescence Dating*, Academic Press, London.
- Aitken, M.J., 1998, *Introduction to Optical Dating: The Dating of Quaternary Sediments by the Use of Photon-stimulated Luminescence*, Oxford University Press, Oxford.
- Ballarini, M., Wallinga, J., Wintle, A.G., and Bos, A.J.J., 2007, A modified SAR protocol for optical dating of individual grains from young quartz samples, *Radiation Measurements*, v. 42, p. 360-369.
- Bøtter-Jensen, L., Bulur, E., Duller, G.A.T. and Murray, A.S., 2000, Advances in luminescence instrument systems, *Radiation Measurements*, v. 32, p. 57-73.
- Briesmeister, J.F., 2000., MCNP – A General Monte Carlo N-Particle Transport Code Version 4C, Report LA-13709-M, Los Alamos National Laboratory, USA.
- Cunningham, A.C., and Wallinga, J., 2010, Selection of integration time intervals for quartz OSL decay curves, *Quaternary Geochronology*, v. 5, p. 657-666.
- Galbraith, R.F., Roberts, R.G., Laslett, G.M., Yoshida, H., and Olley, J.M., 1999, Optical dating of single and multiple grains of quartz from Jinmium rock shelter, northern

- Australia, part 1, Experimental design and statistical models, *Archaeometry*, v. 41, p. 339-364.
- Li, B., 2007, A note on estimating the error when subtracting background counts from weak OSL signals, *Ancient TL*, v. 25, p. 9-14.
- Maigne, L., Perrot, Y., Schaart, D.R., Donnarieix, D. and Breton, V., 2011, Comparison of GATE/GEANT4 with EGSnrc and MCNP for electron dose calculations at energies between 15 keV and 20 MeV, *Physics in Medicine and Biology*, v. 56, p. 811-827.
- Mejdahl, V., 1979, Thermoluminescence dating: beta-dose attenuation in quartz grains, *Archaeometry*, v. 21, p. 31-72.
- Murray, A.S., and Wintle, A.G., 2000, Luminescence dating of quartz using an improved single-aliquot regenerative-dose protocol, *Radiation Measurements*, v. 32, p. 57-73.
- Murray, A.S., and Wintle, A.G., 2003, The single aliquot regenerative dose protocol: potential for improvements in reliability, *Radiation Measurements*, v. 37, p. 377-381.
- Schaart, D.R., Jansen, J.T.M., Zoetelief, J. and de Leege, P.F.A., 2002a, A comparison of MCNP4C electron transport with ITS 3.0 and experiment at incident energies between 100 keV and 20 MeV: influence of voxel size, substeps and energy indexing algorithm, *Physics in Medicine and Biology*, v. 47, p. 1459-1484.
- Schaart, D.R., Bos A.J.J., Winkelman, A.J.M. and Clarijs, M.C., 2002b, The radial depth-dose distribution of a  $^{188}\text{W}/^{188}\text{Re}$  line source measured with novel, ultra-thin TLDs in a PMMA phantom: Comparison with Monte Carlo simulations, *Physics in Medicine and Biology*, v. 47, p. 3605-3627.
- Vandenberghe, D., De Corte, F., Buylaert, J.-P., Kučerac, J., and Van den haute, P., 2008, On the internal radioactivity in quartz, *Radiation Measurements*, v. 43, p. 771-775.
- Wallinga, J., Hobo, N., Cunningham, A.C., Versendaal, A.J., Makaske, B., and Middelkoop, H., 2010, Sedimentation rates on embanked floodplains determined through quartz optical dating, *Quaternary Geochronology*, v. 5, p. 170-175.
- Weerts, H.J.T., 1996, Complex confining layers: Architecture and hydraulic properties of the Holocene and Late Weichselian deposits in the fluvial Rhine-Meuse delta, The Netherlands, PhD thesis, University of Utrecht.

## Captions for Data Repository Figures and Tables

Figure DR1. Thermal transfer tests carried out on selected samples from all sections.

Figure DR2. Results of a preheat-plateau test carried out on sample HK7-1. The ‘central age’  $D_e$  was calculated using the central age model, using only the aliquots which passed the acceptance criteria.

Figure DR3. Normalised dose recovery results from all samples. Central dose recovery ratio (using the CAM) is  $0.997 \pm 0.005$ ,  $\sigma = 2.2 \pm 0.7 \%$ .

Figure DR4. Visual representations of the geometries used for Monte Carlo simulations of beta-radiation transport. Filled rectangular cuboids represent individual pieces of shell material. (a) The geometry designed for the shell-rich samples HK3-4 and HK3-5. (b) The similar representation of hash-rich sample HK7-6.

Figure DR5. The beta energy spectra used to sample electrons in the Monte Carlo model. Spectra were created using the measured radionuclide concentrations (Table DR4) and isotope data from [www.doseinfo-radar.com](http://www.doseinfo-radar.com).

Figure DR6. Sensitivity analysis of the Monte Carlo simulation of beta-radiation transport. In each panel, the outcome ( $r$ ) of the shell model (left side) or hash model (right side) is plotted as a function of one key parameter. Also shown are the central values used in the models (dotted lines), and the estimated  $1\sigma$  uncertainty regions (shaded areas)

Table DR1. Details of the Optically Stimulated Luminescence measurement protocols used in this study. Minor variations in protocol occur within and across stratigraphic sections.

Table DR2. Comparison of  $D_e$  and  $\sigma$  for two storm-surge samples, using two different combinations of decay-curve integration intervals: Early Background uses 0-0.60 s for the initial signal, and 0.60 – 2.10 s for the background subtraction. The Late Background intervals are 0-0.30 s and 36 – 40 s.

Table DR3. Summary of results. Within each section, samples are listed in stratigraphical order (youngest to oldest).  $D_e$  calculated using the Central Age Model (CAM) unless stated. The mean  $\dot{D}$  is given, for details see DR Methods. NAP is the ordnance datum in the Netherlands. Shading indicates samples taken directly from storm-surge units.

Table DR4. Measured radionuclide concentrations determined through high-resolution gamma spectrometry, used as input in Monte Carlo modelling of energy deposition. Sample HK3-3 is the dune sample immediately above the shell layer in section HK3; A separate measurement was made on a sample of pure shells from the HK3 shell layer.

Figure DR1

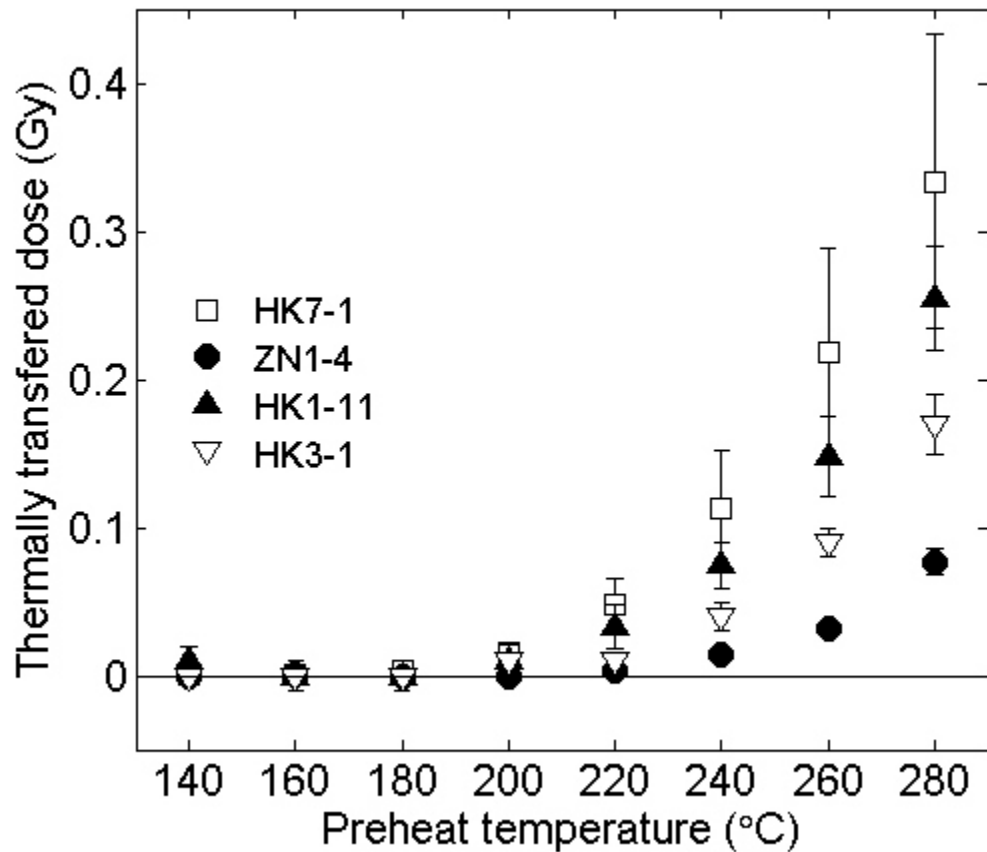


Figure DR2

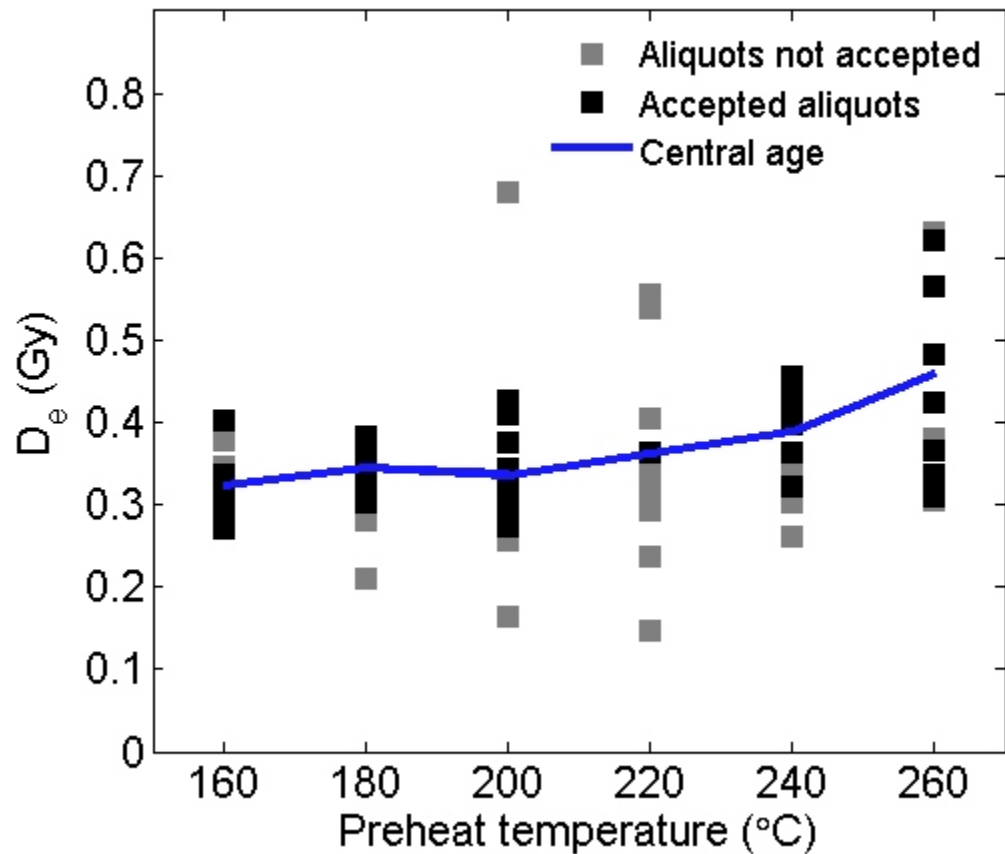




Figure DR4

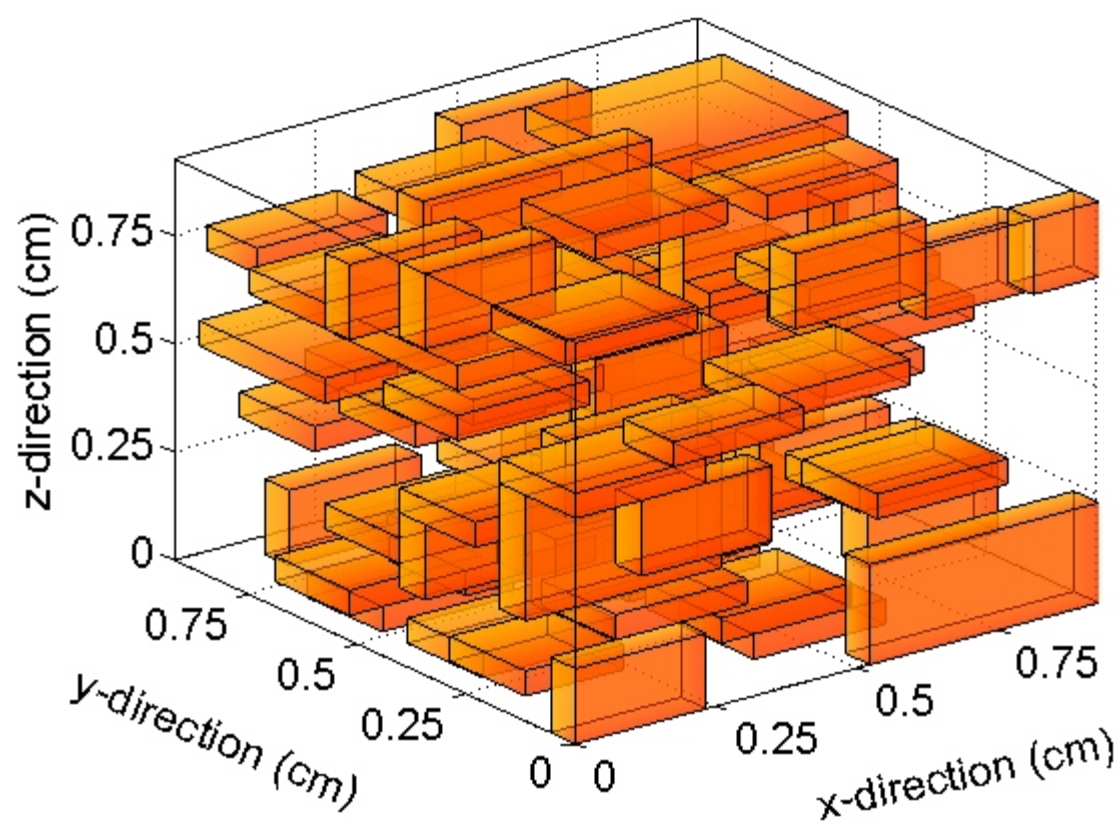
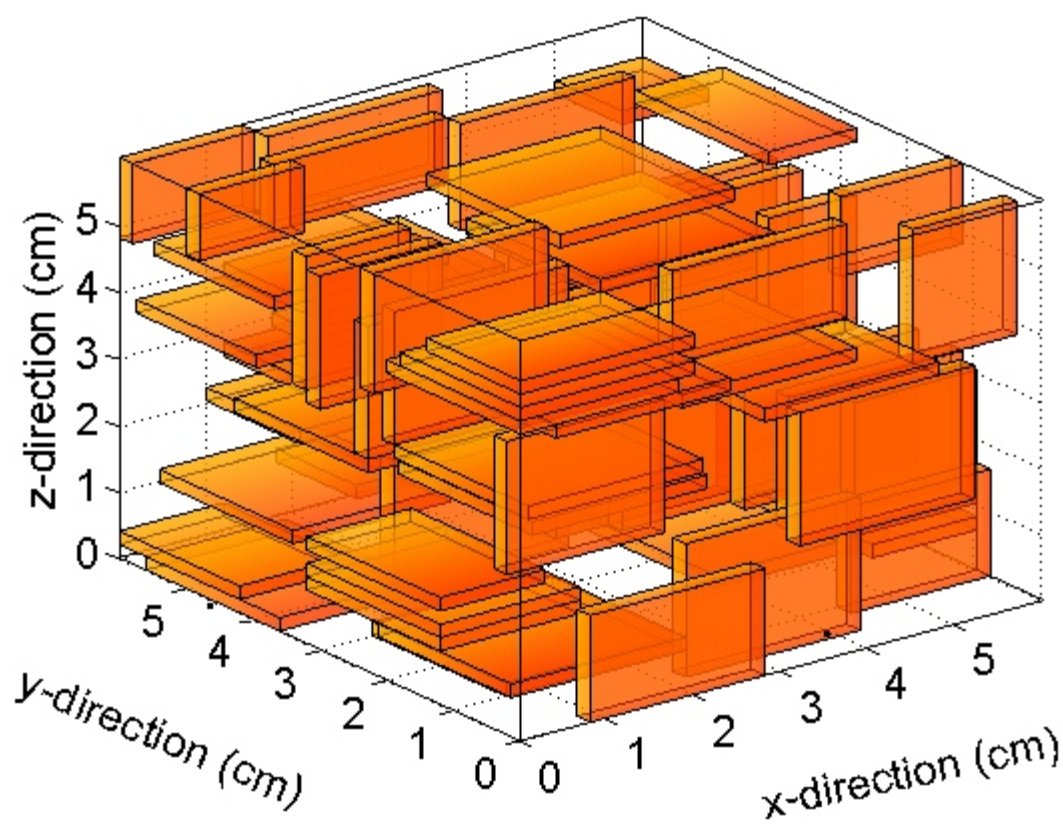


Figure DR5

# Beta Spectra

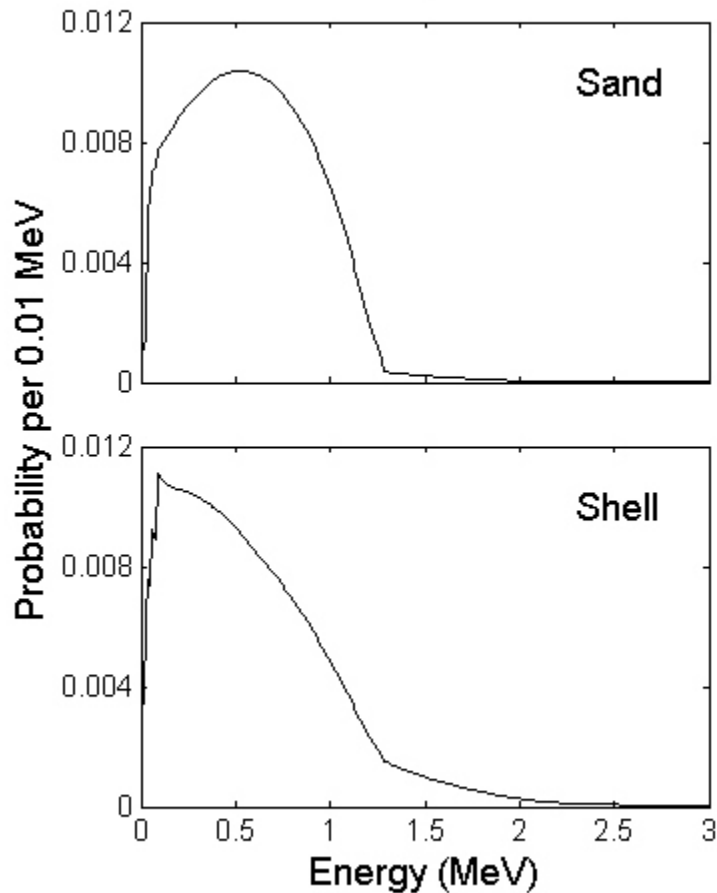
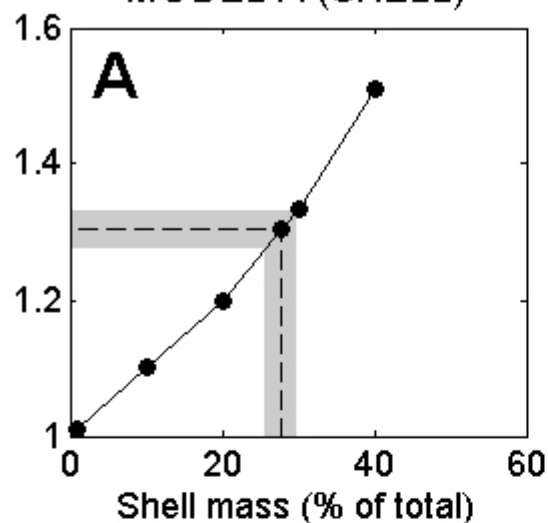
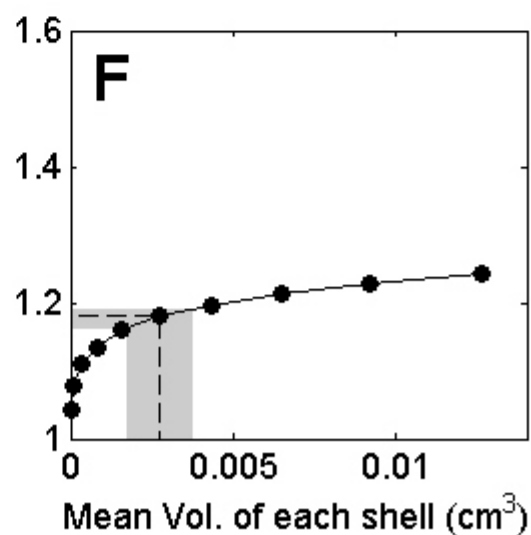
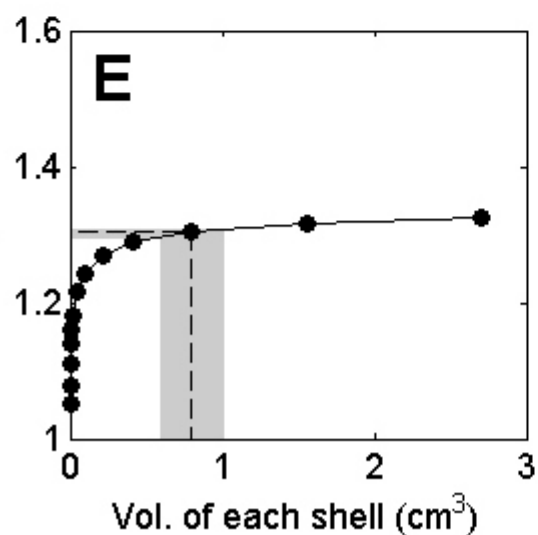
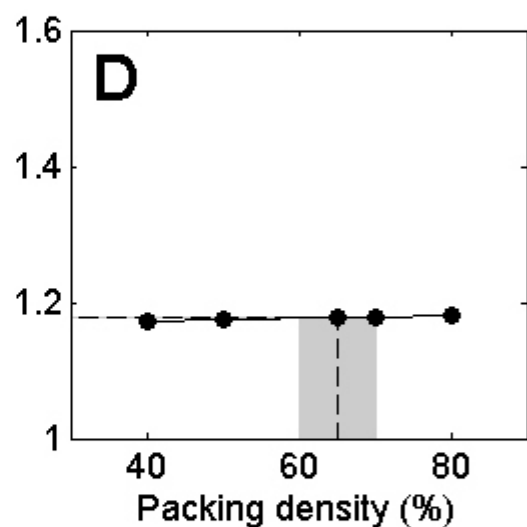
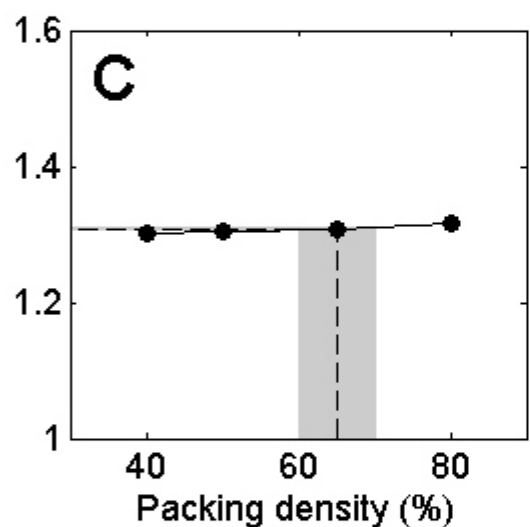
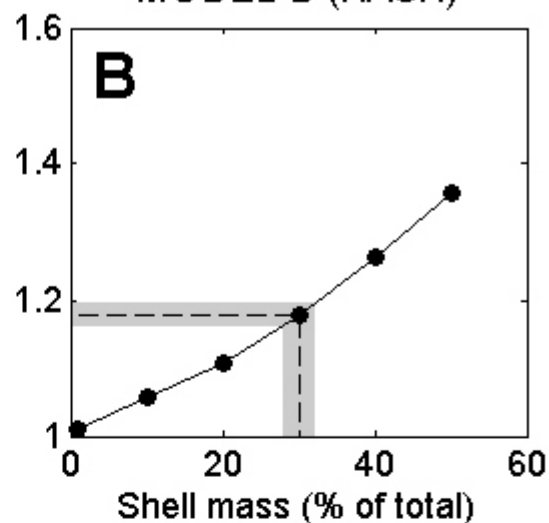


Figure DR5

MODEL A (SHELL)



MODEL B (HASH)



**TABLE DR1.**

<i>Step</i>	<i>HK1<sup>a</sup></i>		<i>HK3</i>	<i>HK7<sup>a</sup></i>		<i>ZN1</i>
Dose	Nat, 2.5, 0, 2.5, 2.5 Gy	Nat, 2.5, 0, 2.5, 2.5 Gy	Nat, 2.1, 0, 2.1 Gy	Nat, 2.5, 0, 2.5, 2.5 Gy	Nat, 2.5, 0, 2.5, 2.5 Gy	Nat, 2.5, 0, 2.5, 2.5 Gy
Preheat	180°C for 10 s	180°C for 10 s	180°C for 10 s	180°C for 10 s	180°C for 10 s	180°C for 10 s
OSL	125°C for 40 s	125°C for 40 s	125°C for 40 s	125°C for 40 s	125°C for 40 s	125°C for 40 s
Test dose	2.5 Gy	2.5 Gy	2.1 Gy	2.5 Gy	2.5 Gy	2.5 Gy
Cutheat	180°C	170°C	180°C	180°C	170°C	170°C
OSL	125°C for 40 s	125°C for 40 s	125°C for 40 s	125°C for 40 s	125°C for 40 s	125°C for 40 s
Bleach	220°C for 40 s	180°C for 40 s	200°C for 40 s	220°C for 40 s	180°C for 40 s	180°C for 40 s

<sup>a</sup>For sections HK1 and HK7, two different protocols were used. There was no effect when slight changes in preheat and high-temperature bleach conditions were made, so all results are include in the analysis.

**TABLE DR2.**

	<i>Early background</i>		<i>Late background</i>	
	<i>De</i>	$\sigma$	<i>De</i>	$\sigma$
<i>HK1-16</i>	$0.34 \pm 0.01$	$0.17 \pm 0.03$	$0.36 \pm 0.01$	$0.21 \pm 0.03$
<i>ZN1-4</i>	$0.36 \pm 0.02$	$0.20 \pm 0.04$	$0.43 \pm 0.03$	$0.33 \pm 0.05$

TABLE DR3.

Section	Sample No.	Height NAP (m)	$D_e$ (Gy)	$\sigma$	No. aliquots	Dose rate (Gy ka <sup>-1</sup> )	Age (ka)	Year AD	footnotes
HK1	2	8.43	0.137 ± 0.004	0.134 ± 0.028	32	1.136 ± 0.05	0.121 ± 0.007	<b>1887 ± 7</b>	
	4	7.33	0.141 ± 0.005	0.157 ± 0.032	31	1.11 ± 0.05	0.127 ± 0.008	<b>1881 ± 8</b>	
	8	6.53	0.296 ± 0.006	0.141 ± 0.018	65	1.242 ± 0.05	0.238 ± 0.012	<b>1770 ± 12</b>	a
	11	6.13	0.285 ± 0.009	0.148 ± 0.025	40	1.197 ± 0.05	0.238 ± 0.013	<b>1770 ± 13</b>	
	14	5.93	0.289 ± 0.006	0.114 ± 0.018	52	1.268 ± 0.05	0.228 ± 0.011	<b>1780 ± 11</b>	
	16	5.68	0.346 ± 0.014	0.168 ± 0.034	25	1.137 ± 0.05	0.304 ± 0.019	<b>1704 ± 19</b>	
	18	5.48	0.397 ± 0.011	0.163 ± 0.021	41	1.259 ± 0.05	0.315 ± 0.017	<b>1693 ± 17</b>	
	21	3.43	0.366 ± 0.011	0.151 ± 0.023	38	0.929 ± 0.04	0.394 ± 0.022	<b>1614 ± 22</b>	
HK3	0	5.91	0.267 ± 0.01	0.11 ± 0.035	20	1.28 ± 0.05	0.208 ± 0.012	<b>1800 ± 12</b>	
	1	5.26	0.275 ± 0.007	0.097 ± 0.023	27	1.275 ± 0.05	0.216 ± 0.011	<b>1792 ± 11</b>	
	2	5.02	0.279 ± 0.01	0.137 ± 0.029	26	1.318 ± 0.05	0.212 ± 0.012	<b>1796 ± 12</b>	
	3	4.84	0.275 ± 0.007	0.051 ± 0.032	18	1.207 ± 0.05	0.228 ± 0.012	<b>1780 ± 12</b>	
	4	4.69	0.233 ± 0.008	0.137 ± 0.029	36	0.989 ± 0.05	0.236 ± 0.015	<b>1772 ± 15</b>	b,c
	5	4.69	0.238 ± 0.008	0.106 ± 0.03	24	1.039 ± 0.05	0.229 ± 0.014	<b>1779 ± 14</b>	b,c
	7	4.49	0.427 ± 0.017	0.138 ± 0.032	17	1.254 ± 0.05	0.341 ± 0.02	<b>1667 ± 20</b>	
	8	4.25	0.411 ± 0.016	0.171 ± 0.031	25	1.101 ± 0.05	0.373 ± 0.024	<b>1635 ± 24</b>	
	9	4.00	0.403 ± 0.011	0.118 ± 0.023	35	1.204 ± 0.05	0.334 ± 0.018	<b>1674 ± 18</b>	
	10	3.68	0.399 ± 0.011	0.083 ± 0.026	16	1.163 ± 0.05	0.343 ± 0.019	<b>1665 ± 19</b>	
	11	3.13	0.408 ± 0.009	0.067 ± 0.021	21	1.289 ± 0.05	0.317 ± 0.015	<b>1691 ± 15</b>	
HK7	10	6.26	0.273 ± 0.01	0.143 ± 0.03	23	1.2 ± 0.05	0.228 ± 0.013	<b>1780 ± 13</b>	
	9	5.91	0.268 ± 0.008	0.164 ± 0.023	77	1.072 ± 0.05	0.25 ± 0.015	<b>1758 ± 15</b>	
	7	5.46	0.325 ± 0.005	0.079 ± 0.013	54	1.237 ± 0.05	0.262 ± 0.012	<b>1746 ± 12</b>	
	6	5.31	0.259 ± 0.008	0.13 ± 0.025	32	0.996 ± 0.04	0.26 ± 0.014	<b>1748 ± 14</b>	a,b,c
	5	5.16	0.335 ± 0.007	0.149 ± 0.017	69	1.278 ± 0.05	0.262 ± 0.013	<b>1746 ± 13</b>	
	4	4.91	0.34 ± 0.007	0.119 ± 0.018	47	1.304 ± 0.05	0.261 ± 0.013	<b>1747 ± 13</b>	
	1	5.36	0.338 ± 0.009	0.147 ± 0.02	44	1.185 ± 0.05	0.285 ± 0.015	<b>1723 ± 15</b>	
	3	4.41	0.351 ± 0.009	0.149 ± 0.021	35	1.2 ± 0.05	0.292 ± 0.015	<b>1716 ± 15</b>	
	2	3.86	0.342 ± 0.009	0.134 ± 0.022	44	1.166 ± 0.05	0.293 ± 0.016	<b>1715 ± 16</b>	
ZN1	5	2.08	0.302 ± 0.007	0.106 ± 0.021	23	1.314 ± 0.04	0.23 ± 0.01	<b>1778 ± 10</b>	d
	4	1.95	0.304 ± 0.013	0.100	23	1.286 ± 0.04	0.236 ± 0.014	<b>1772 ± 14</b>	e
	3	1.83	1.131 ± 0.016	0.029 ± 0.017	14	1.322 ± 0.04	0.855 ± 0.034	<b>1153 ± 34</b>	
	2	1.71	1.072 ± 0.025	0.098 ± 0.019	27	1.344 ± 0.042	0.797 ± 0.035	<b>1211 ± 35</b>	

a excludes 1 high outlier

b beta dose corrected for non-uniform matrix

c gamma dose corrected for non-infinite matrix

d excludes 2 high outliers

e MAM3 used for  $D_e$  estimate, using  $\sigma = 0.10$

**TABLE DR4.**

	<i>Radionuclide concentration (Bq kg<sup>-1</sup>)</i>		
	<sup>40</sup> K	<sup>238</sup> U	<sup>232</sup> Th
Sand fraction (HK3-3)	320 ± 5	6.58 ± 0.15	6.24 ± 0.33
Shells only	3.0 ± 1.6	1.0 ± 0.1	0.27 ± 0.03